Journal of Inorganic Biochemistry 122 (2013) 49–56

Contents lists available at SciVerse ScienceDirect

Journal of Inorganic Biochemistry

journal homepage: www.elsevier.com/locate/jinorgbio

Impact of metal on the DNA photo-induced cleavage activity of a family of Phterpy complexes

Gong-Jun Chen [a,b], Zhi-Gang Wang [b], Ying-Ying Kou [b], Jin-Lei Tian [b,*], Shi-Ping Yan [b,*]

[a] College of Chemistry, Chemical Engineering and Materials Science, Shandong Normal University, Jinan, 250014, PR China
[b] Department of Chemistry and Key Laboratory of Advanced Energy Materials Chemistry (MOE) and TKL of Metal and Molecule Based Material Chemistry, Nankai University, Tianjin 300071, PR China

ARTICLE INFO

Article history:
Received 8 October 2012
Received in revised form 12 January 2013
Accepted 16 January 2013
Available online 26 January 2013

Keywords:
Crystal structures
DNA binding
Photo-induced DNA cleavage

ABSTRACT

A family of Phterpy complexes, $[Mn(Phterpy)_2][N(CN)_2]_2\cdot 0.5H_2O$ (**1**), $[Fe(Phterpy)_2](NO_3)_2$ (**2**), $[Ni(Phterpy)_2](NO_3)_2$ (**3**), $[Ni(Phterpy)_2]Cl_2\cdot 10H_2O$ (**4**), $[Cd(Phterpy)_2](NO_3)_2\cdot 2H_2O$ (**5**) and $[Zn(Phterpy)Cl_2]$ (**6**) (Phterpy = 4′-phenyl-2,2′:6′,2″-terpyridine), have been synthesized and structurally characterized, and their DNA binding and photo-induced DNA cleavage activities have been investigated. These complexes display binding propensity to the CT-DNA giving a relative order: **1**>**4**>**3**, **5**, **2**, **6**. Under dark or ambient lighting conditions, all complexes show no efficient DNA cleavage activity to pBR322 DNA. While on irradiation with UV-A light of 365 nm, complexes of **1**, **3** and **4** exhibit significant cleavage activities. In the presence of H_2O_2 as a revulsant or an activator, the cleavage ability of complex **2** is obviously enhanced. Complexes **5** and **6** do not exhibit any apparent chemical nuclease activities under irradiation conditions or with the addition of H_2O_2. The DNA photo-induced cleavage activities are consistent with the number of single-electron in the central metal ion of complexes and singlet oxygen and hydroxyl radical are found as the reactive oxygen species.

1. Introduction

Photo-induced DNA cleavage involves the simultaneous presence of light, oxygen, and photosensitizing drugs to achieve the photo cytotoxic effect, among which electron transfer and energy transfer are the two most prevalent processes. Transition metal complexes that are capable of cleaving DNA under physiological conditions are of current interest in the development of metal-based anticancer agents [1–7]. It inspires inorganic chemists to develop more effective, less toxic, target specific, and preferably noncovalently bound anticancer drugs [8–18]. Photo-induced DNA cleavage as a nontoxic and high selective modality for treatment of solid tumors has attracted increasing attention [19–26]. The methodology based on irradiation with UV-A light has achieved much success for its potential in the treatment of tumor combined with light and a photosensitizing drug among many methodologies used for oxidative cleavage of DNA [27]. Complexes based on the planar heterocyclic ligands have been well investigated due to their unusual electronic properties, diverse chemical reactivity and peculiar structure [19–26,28–47]. The ligand 4′-phenyl-2,2′:6′,2″-terpyridine (Phterpy) has a larger aromatic ring used to generate photo-induced $^3(n–\pi)$ and/or $^3(\pi–\pi)$ states that can transfer its excited state energy to molecular oxygen in a type-II process forming singlet oxygen with oxidative damage to cells. Moreover, less report has focused on the photo-induced DNA cleavage with the influence of the different transition metals. In attempt to obtain more insight on the selectivity and efficiency of DNA cleavage with different transition metal complexes, herein we prepared a series of mononuclear d-metal complexes and investigated their DNA cleavage activities.

2. Experimental

2.1. Materials and measurements

The ligand Phterpy was synthesized according to a previous reported procedure [48,49]. Ethidium bromide (EB), calf thymus DNA (CT-DNA) and pBR322 plasmid DNA were purchased from Sigma. A Tris–HCl buffer solution was prepared using deionized sonicated and triple-distilled water. All other reagents and chemicals were purchased from commercial sources and used as received. Elemental analyses for C, H and N were obtained on a Perkin-Elmer analyzer model 240. The electronic spectra were measured on a JASCO V-570 spectrophotometer. The CD spectra of CT-DNA in the presence or absence of a complex were collected in a 5 mM Tris–HCl buffer (pH = 7.2) containing 50 mM NaCl. All CD experiments were performed on a JASCO-J715 spectropolarimeter at room temperature.

2.2. Synthesis of $[Mn(Phterpy)_2][N(CN)_2]_2\cdot 0.5H_2O$ (1)

An acetonitrile solution (10 mL) of $MnCl_2\cdot 6H_2O$ (0.2 mmol, 43 mg) was added to a 10 mL methanol/H_2O (1:1) mixture of Phterpy (0.2 mmol, 62.6 mg) and $NaN(CN)_2$ (0.2 mmol, 18 mg). The resulting

* Corresponding authors. Tel.: +86 22 23509957; fax: +86 22 23502779.
E-mail addresses: tiant@nankai.edu.cn (J.-L. Tian), yansp@nankai.edu.cn (S.-P. Yan).

0162-0134/$ – see front matter © 2013 Elsevier Inc. All rights reserved.
http://dx.doi.org/10.1016/j.jinorgbio.2013.01.010

mixture was stirred for 3 h at room temperature and then filtered. Several weeks later, the yellow block crystals suitable for X-ray diffraction were obtained by slow evaporation of the filtrate. Yield: 24% (based on the $MnCl_2 \cdot 6H_2O$ solution). Elemental analysis data: calcd. (%) for $C_{46}H_{31}MnN_{12}O_{0.50}$: C, 67.81; H, 3.84; N, 20.63; found (%): C, 67.82; H, 3.85; N, 20.61.

2.3. Synthesis of $[Fe(Phterpy)_2](NO_3)_2$ (**2**)

An acetonitrile solution (10 mL) of $Fe(NO_3)_2 \cdot 6H_2O$ (0.2 mmol, 57 mg) and ascorbic acid (0.3 mmol, 53 mg) were added to a 10 mL methanol/H_2O (1:1) mixture of Phterpy (0.2 mmol, 62.6 mg). The resulting mixture was stirred for 2 h at room temperature and then filtered. Green block crystals suitable for X-ray diffraction were obtained by slow evaporation of the filtrate after several weeks. Yield: 35% (based on the $Fe(NO_3)_2 \cdot 6H_2O$ solution). Elemental analysis data: calcd. (%) for: $C_{42}H_{30}FeN_8O_6$: C, 63.17; H, 3.79; N, 14.03; found (%): C, 63.17; H,3.82; N, 14.01.

2.4. Synthesis of $[Ni(Phterpy)_2](NO_3)_2$ (**3**)

Complexes **3** and **4** were prepared according to the literature methods [49,50]. An acetonitrile solution (10 mL) of $Ni(NO_3)_2 \cdot 6H_2O$ (0.2 mmol, 58 mg) was added to a 10 mL methanol/H_2O (1:1) mixture of Phterpy (0.2 mmol, 62.6 mg). The resulting mixture was stirred for 2 h at room temperature and then filtered. Green block crystals suitable for X-ray diffraction were obtained by slow evaporation of the filtrate after several weeks. Yield: 50% (based on the $Ni(NO_3)_2 \cdot 6H_2O$ solution). Elemental analysis data: calcd. (%) for $C_{42}H_{30}NiN_8O_6$: C, 62.94; H, 3.77; N, 13.98; found (%): C, 62.95; H, 3.79; N, 13.96.

2.5. Synthesis of $[Ni(Phterpy)_2]Cl_2 \cdot 10H_2O$ (**4**)

Complex **4** was prepared similar to **3**, but 0.2 mmol $NiCl_2 \cdot 6H_2O$ instead of $Ni(NO_3)_2 \cdot 6H_2O$ was added to the reaction mixture. Then green block crystals suitable for X-ray diffraction were obtained by slow evaporation of the filtrate after several months. Yield: 43% (based on the $NiCl_2 \cdot 6H_2O$ solution). Elemental analysis data: calcd. (%) for: $C_{42}H_{50}N_6NiCl_2O_{10}$: C, 54.33; H, 5.43; N, 9.05; found (%): C, 54.34; H, 5.45; N, 9.08.

2.6. Synthesis of $[Cd(Phterpy)_2](NO_3)_2 \cdot 2H_2O$ (**5**)

Complex **5** was prepared similar to **3**, but 0.2 mmol $Cd(NO_3)_2 \cdot 6H_2O$ instead of $Ni(NO_3)_2 \cdot 6H_2O$ was added to the reaction mixture. Then colorless block crystals suitable for X-ray diffraction were obtained by slow evaporation of the filtrate after several months. Yield: 35% (based on the $Cd(NO_3)_2 \cdot 6H_2O$ solution). Elemental analysis data: calcd. (%) for: $C_{42}H_{34}CdN_8O_8$: C, 56.60; H, 3.85; N, 12.57; found (%): C, 56.55; H, 3.87; N, 12.60.

2.7. Synthesis of $[Zn(Phterpy)Cl_2]$ (**6**)

Complex **6** was prepared similar to **3**, but 0.2 mmol $ZnCl_2 \cdot 6H_2O$ instead of $Ni(NO_3)_2 \cdot 6H_2O$ was added to the reaction mixture. Then colorless block crystals suitable for X-ray diffraction were obtained by slow evaporation of the filtrate after several months. Yield: 35% (based on the $ZnCl_2 \cdot 6H_2O$ solution). Elemental analysis data: calcd. (%) for: $C_{21}H_{15}Cl_2N_3Zn$: found (%): C, 56.59; H, 3.39; N, 9.43; found (%): C, 56.57; H, 3.44; N, 9.40.

2.8. X-ray crystallography

Diffraction data for **1**–**6** were collected at 293 (2) K, with a Bruker Smart 1000 CCD diffractometer using Mo-Kα radiation (λ = 0.71073 Å) with the ω-2θ scan technique. An empirical absorption correction was applied to raw intensities [51]. The structures were solved by direct methods (SHELX-97) and refined with full-matrix least-squares technique on F^2 using the SHELX-97 [52,53]. The hydrogen atoms were added theoretically, and riding on the concerned atoms and refined with fixed thermal factors. The details of the crystallographic data and structure refinement parameters are summarized in Table 1. The crystallographic data for complexes **1**–**6** have been deposited with the Cambridge Crystallographic Data Centre with the corresponding CCDC numbers of 632172 (**1**), 294395 (**2**), 288966 (**3**), 632171 (**4**), 292420 (**5**) and 675399 (**6**). Copy of the data can be obtained free of charge on application to CCDC, e-mail: deposit@ccdc.cam.ac.uk or http://www.ccdc.cam.ac.uk.

2.9. DNA-binding and cleavage experiments

The UV absorbance at 260 nm and 280 nm of the CT-DNA solution in 18 mM NaCl/50 mM Tris–HCl buffer (pH = 7.2) gives a ratio of 1.8–1.9, indicating that the DNA was sufficiently free of protein. The concentration of CT-DNA was determined from its absorption intensity at 260 nm with a molar absorptivity of 6600 M^{-1} cm^{-1} [54,55]. DNA binding experiments were done in Tris–HCl/NaCl buffer (50 mM Tris–HCl, 18 mM NaCl, pH = 7.2) using the aqueous solution of the complexes. Absorption titration experiments were made by varying the concentration of CT-DNA while keeping the metal complex concentration constant. Each spectrum of the complexes binding to DNA was recorded after equilibration of the sample for 5 min at 25 °C.

The relative bindings of the complexes to CT-DNA were studied with an EB–DNA solution in Tris–HCl/NaCl buffer (pH = 7.2). The experiment was carried out by titrating complexes into the EB–DNA solution containing 4.0×10^{-6} M of EB and 8.0×10^{-6} M of DNA. The fluorescence spectra were recorded at room temperature with excitation at 510 nm and emission at 602 nm.

The DNA cleavage experiments were done by agarose gel electrophoresis, which was performed by incubation at 37 °C as follows: pBR322 DNA in a 50 mM Tris–HCl/18 mM NaCl buffer (pH = 7.2) was treated with the complexes in the absence of additives. The samples were incubated with light irradiation, and then a loading buffer was added. Then the samples were electrophoresed for 3 h at 80 V on 0.8% agarose gel using a Tris–boric acid–EDTA buffer. After electrophoresis, bands were visualized by UV-A light and photographed. Quantification of cleavage products was performed by UVIpro software, version 10.03. Supercoiled plasmid DNA values were corrected by a factor of 1.3, based on the average literature estimate of lowered binding of ethidium [56–58].

Cleavage mechanistic investigations of pBR322 DNA were done by adding different reagents such as DMSO, NaN_3, SOD, KI, EDTA, EtSH, histidine, D_2O and catalase to pBR322 DNA prior to the addition of the complexes. Deoxygenated solutions were prepared by four freeze–pump–thaw cycles. Before each cycles the solutions were equilibrated with nitrogen to aid the deoxygenation process. The deoxygenated solutions were stored under a nitrogen atmosphere prior to use.

3. Results and discussion

3.1. Crystal structures

Complexes **1**–**6** can be divided into three groups according to the space group: (i) *P*-1 triclinic (**1**–**4**), (ii) *P*bca orthorhombic (**5**) and (iii) *P*2(1)/n monoclinic (**6**). The bond lengths and angles for the coordination spheres are given in Table 2. For **1**–**5**, all M(II) centers adopt distorted octahedron coordination environments and each Phterpy ligand coordinates the M(II) center in a *mer* fashion defining essentially tetragonally compressed $[MN_6]$ octahedrons. The M – N axial bonds involving the pyridine rings are markedly shorter than the M – N equatorial bonds collectively denoted as $M-N_{central}$ and

Table 1
Data collection and processing parameters for complexes **1**–**6**.

Complex	**1**	**2**	**3**	**4**	**5**	**6**
Empirical formula	$C_{46}H_{31}MnN_{12}O_{0.50}$	$C_{42}H_{30}N_8NiO_6$	$C_{42}H_{50}Cl_2N_6NiO_{10}$	$C_{42}H_{30}FeN_8O_6$	$C_{42}H_{34}CdN_8O_8$	$C_{21}H_{15}Cl_2N_3Zn$
Formula weight	814.77	801.45	928.49	798.59	891.17	445.63
Temperature (K)	113(2)	293(2)	113(2)	293(2)	293(2)	113(2)
Wavelength (Å)	0.71073	0.71073	0.71073	0.71073	0.71073	0.71073
Crystal system	Triclinic	Triclinic	Triclinic	Triclinic	Orthorhombic	Monoclinic
Space group	*P*-1	*P*-1	*P*-1	*P*-1	*Pbca*	*P*2(1)/*n*
Unit cell dimensions						
(Å)	8.767(3)	9.0410(15)	10.190(2)	9.095(3)	10.7823(13)	11.963(2)
a (Å)	13.821(4)	11.0427(19)	12.154(2)	10.968(4)	16.9764(19)	9.5370(19)
b (Å)	16.501(5)	20.198(3)	19.783(5)	20.236(6)	42.788(5)	17.124(3)
c (Å)	86.217(12)	94.444(3)	74.728(9)	94.647(6)	90	90
α (°)	76.567(7)	100.745(3)	87.303(11)	101.033(5)	90	108.56(3)
β (°)	89.172(11)	106.380(3)	67.009(7)	106.389(6)	90	90
γ (°)						
V (Å^3)	1940.4(10)	1882.6(5)	2171.6(8)	1881.2(10)	7832.1(16)	1852.2(6)
Z	2	2	2	2	8	4
ρ (mg/m^3)	1.395	1.414	1.420	1.410	1.512	1.598
μ (mm^{-1})	0.394	0.576	0.634	0.462	0.623	1.625
F (000)	840	828	972	824	3632	904
θ range (°) for data collection	1.48 to 26.00	1.94 to 25.01	1.89 to 26.00	1.96 to 25.01	0.95 to 26.42	1.83 to 25.02
Limiting indices	$-10\le h\le 10$, $-17\le k\le 16$, $-20\le l\le 20$	$-10\le h\le 5$, $-11\le k\le 13$, $-24\le l\le 23$	$-12\le h\le 12$, $-14\le k\le 14$, $-24\le l\le 16$	$-10\le h\le 10$, $-7\le k\le 13$, $-24\le l\le 20$	$-13\le h\le 13$, $-12\le k\le 21$, $-52\le l\le 53$	$-14\le h\le 14$, $-11\le k\le 6$, $-20\le l\le 20$
Reflections collected/unique	21,611/7613 [$R_{(int)}=0.0552$]	9592/6551 [$R_{(int)}=0.0283$]	17,953/8463 [$R_{(int)}=0.0299$]	9426/6494 [$R_{(int)}=0.0482$]	42,329/8021 [$R_{(int)}=0.0747$]	10,962/3274 [$R_{(int)}=0.0390$]
Max. and min. transmission	0.9397 and 0.9184	1.000 and 0.7073	0.9393 and 0.8837	1.0000 and 0.7745	0.833 and 0.799	0.8284 and 0.804
Data/restraints/parameters	7613/97/590	6551/54/550	8463/0/552	6494/136/568	8021/136/594	3274/0/244
Goodness-of-fit on F^2	1.070	1.011	1.040	1.038	1.030	1.044
Final *R* indices [$I>2\theta(I)$]	$R_1=0.0732$, $wR_2=0.1996$	$R_1=0.0699$, $wR_2=0.1765$	$R_1=0.0571$, $wR_2=0.1521$	$R_1=0.0833$, $wR_2=0.1927$	$R_1=0.0637$, $wR_2=0.1309$	$R_1=0.0277$,$wR_2=0.0682$
R indices (all data)	$R_1=0.1002$, $wR_2=0.2220$	$R_1=0.1143$, $wR_2=0.2120$	$R_1=0.0699$, $wR_2=0.1649$	$R_1=0.1645$, $wR_2=0.2415$	$R_1=0.1346$, $wR_2=0.1589$	$R_1=0.0313$, $wR_2=0.0708$
Largest diff. peak and hole (e·Å^{-3})	0.851 and −0.401	1.086 and −0.496	1.085 and −0.855	1.003 and −0.611	0.557 and −0.432	0.263 and −0.314

Table 2
Selected bonds lengths (Å) and angles (deg) for complexes **1**–**6**.

1	Mn1 – N1	2.244(3)	Mn1 – N2	2.184(4)
	Mn1 – N3	2.253(3)	Mn1 – N4	2.221(3)
	Mn1 – N5	2.185(3)	Mn1 – N6	2.244(3)
	N1 – Mn1 – N2	72.7(1)	N1 – Mn1 – N3	145.1(1)
	N1 – Mn1 – N4	98.8(1)	N1 – Mn1 – N5	113.3(1)
	N2 – Mn1 – N4	115.0(1)	N2 – Mn1 – N5	170.1(1)
	N3 – Mn1 – N5	101.3(1)	N3 – Mn1 – N6	92.1(1)
2	Fe1 – N1	1.961(5)	Fe1 – N2	1.871(5)
	Fe1 – N3	1.969(5)	Fe1 – N4	1.978(5)
	Fe1 – N5	1.883(5)	Fe1 – N6	1.993(5)
	N1 – Fe1 – N	81.3(2)	N1 – Fe1 – N3	162.0(2)
	N1 – Fe1 – N4	90.1(2)	N1 – Fe1 – N5	100.3(2)
	N2 – Fe1 – N4	97.5(2)	N2 – Fe1 – N5	177.5(2)
	N4 – Fe1 – N5	80.6(2)	N4 – Fe1 – N6	161.3(2)
3	Ni1 – N1	2.121(4)	Ni1 – N2	1.987(4)
	Ni1 – N3	2.116(4)	Ni1 – N4	2.099(4)
	Ni1 – N5	1.996(4)	Ni1 – N6	2.119(5)
	N1 – Ni1 – N3	156.0(2)	N2 – Ni1 – N4	103.1(2)
	N2 – Ni1 – N5	177.4(2)	N2 – Ni1 – N6	100.9(2)
	N3 – Ni1 – N5	99.6(2)	N3 – Ni1 – N6	92.0(2)
4	Ni1 – N	2.098(3)	Ni1 – N2	1.982(3)
	Ni1 – N3	2.106(3)	Ni1 – N4	2.105(3)
	Ni1 – N5	1.977(2)	Ni1 – N6	2.105(3)
	N1 – Ni1 – N2	78.7(1)	N1 – Ni1 – N3	156.7(1)
	N1 – Ni1 – N4	94.1(1)	N1 – Ni1 – N5	99.7(1)
	N2 – Ni1 – N5	178.1(1)	N4 – Ni1 – N6	156.5(1)
5	Cd1 – N1	2.333(5)	Cd1 – N2	2.287(4)
	Cd1 – N3	2.376(5)	Cd1 – N4	2.341(5)
	Cd1 – N5	2.307(4)	Cd1 – N6	2.355(5)
	N1 – Cd1 – N2	70.5(2)	N1 – Cd1 – N3	139.6(2)
	N1 – Cd1 – N4	96.1(2)	N1 – Cd1 – N5	121.4(2)
	N1 – Cd1 – N6	100.0(2)	N2 – Cd1 – N3	69.9(2)
	N2 – Cd1 – N4	120.9(2)	N2 – Cd1 – N5	164.4(2)
6	Zn1 – N1	2.1886(19)	Zn1 – N2	2.0940(19)
	Zn1 – N3	2.1913(18)	Zn1 – Cl1	2.2650(7)
	Zn1 – Cl2	2.2686(7)	N1 – Zn1 – N2	74.55(7)
	N1 – Zn1 – N3	149.20(7)	N2 – Zn1 – N3	74.67(7)
	N1 – Zn1 – Cl1	96.97(5)	N1 – Zn1 – Cl2	99.10(5)
	N2 – Zn1 – Cl1	124.60(5)	N2 – Zn1 – Cl2	118.74(5)

$N-N_{distal}$, respectively. It is worthwhile mentioning that complex **6** has distorted trigonal bipyramidal geometry. In all complexes, aromatic Phterpy ligands tend to self-assemble via intermolecular π–π interactions as shown in Fig. 1.

3.1.1. $[Mn(Phterpy)_2][N(CN)_2]_2 \cdot 0.5H_2O$ (**1**)

The Mn(II) center is in a distorted octahedral geometry owing to the rotation of pyridine rings within a Phterpy ligand. The angle of N(2) – Mn – N(5) is 170.14°, thus the two terpyridines are tilted 9.86° away from perfect orthogonality. The Mn – N(2) and Mn – N(5) axial bonds involving the pyridine rings are markedly shorter than the equatorial bonds [Mn – N(1), Mn – N(3), Mn – N(4) and Mn – N(6)]. The crystal structure of **1** is shown in Fig. 2. The average bond of Mn(II) – N

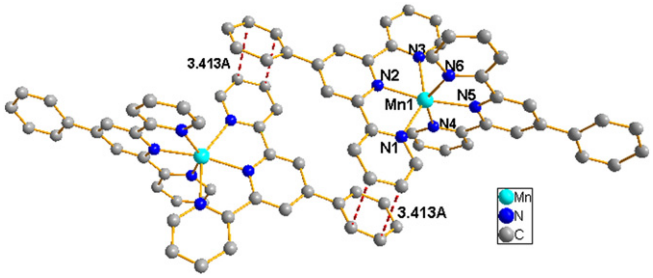

Fig. 2. Perspective view of **1** cation with the atom-numbering scheme. Hydrogen atoms and environmental anions are omitted for clarity.

is 2.222(4) Å, which is slightly shorter than the average Mn(II) – N bond length of 2.27 Å observed for the monocationic $[Mn(py_5)Cl]^+$ unit [59], but still consistent with a high-spin Mn(II) center [60].

3.1.2. $[Fe(Phterpy)_2](NO_3)_2$ (**2**)

The structure of complex **2** is shown in Fig. 3. Complex **2** has a distorted octahedral geometry; two terpyridines are tilted 2.5° close to perfect orthogonality. The Fe – N(2) and Fe – N(5) axial bonds involving the pyridine rings are markedly shorter than the equatorial bonds [Fe – N(1), Fe – N(3), Fe – N(4) and Fe – N(6)]. The metal–nitrogen distances are obviously shorter than in complex **1** with an average Fe – N bond length of 1.942(5) Å within the range of 1.938(2)–2.042(2) Å [61]. The shorter bond lengths may result from the low-spin state of the metal ion [62]. The shorter bond to the central pyridine nitrogens also allows for *cis* N–Fe–N angles that are much closer to the idealized octahedral values. Moreover, there are strong intermolecular π–π interactions between ligand layers (π-stacking overlap), while there are no intramolecular π–π interactions.

3.1.3. $[Ni(Phterpy)_2](NO_3)_2$ (**3**) and $[Ni(Phterpy)_2]Cl_2 \cdot 10H_2O$ (**4**)

The Ni – N (axial) and Ni – N (equatorial) bond lengths of **4** are markedly shorter than that of **3**. The average Ni – N bond lengths of **3** and **4** are 2.073(1) and 2.062(2) Å, respectively. The axial positions are occupied by the atoms of N(5) and N(2) with the angles of N2–Ni1–N5 equal to 177.42° (**3**) and 178.03° (**4**). For **4**, two terpyridines are tilted 1.97° and can be seen at an almost perfect orthogonality. The structure of complexes **3** and **4** contains layers of the 2D-Phterpy embrace, each of which interacts with neighboring layers only through edge-to-face interactions between phenyl groups (Figs. 4, 5.) [63]. In addition, there are complicated hydrogen bonding interactions in **4**, which enhance the stability of the crystal structure.

3.1.4. $[Cd(Phterpy)_2](NO_3)_2 \cdot 2H_2O$ (**5**)

The coordination sphere for **5** is also a distorted octahedron with the average Cd – N bond length of 2.333(2) Å.

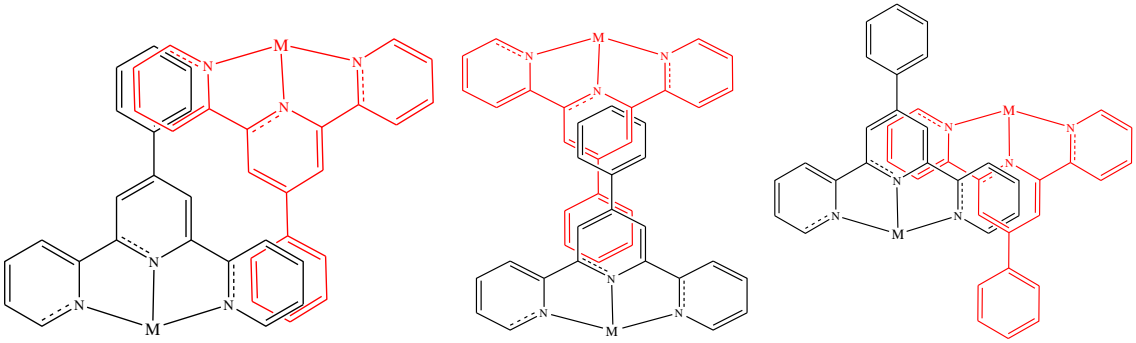

Fig. 1. Some of the possible crystal packing interactions for complexes with Phterpy ligands.

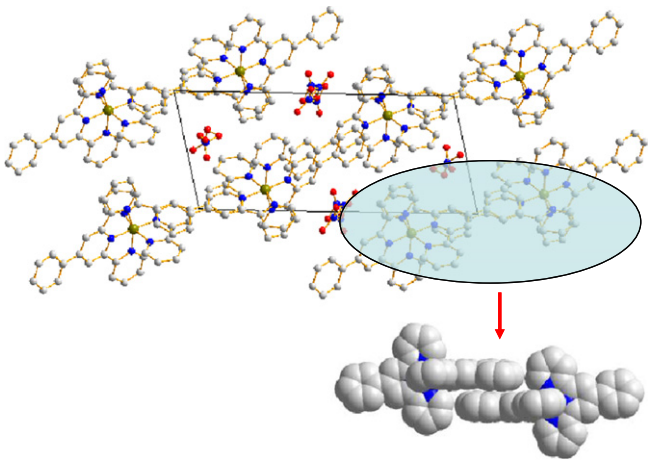

Fig. 3. Packing diagram within the layer of **2** and face-to-face of the ligand interactions in **2**.

3.1.5. [Zn(Phterpy)Cl_2] (**6**)

The molecular structure of **6** is shown in Fig. 6. It crystallizes in the monoclinic space group *P*2(1)/n. The geometry of the complex is best described as trigonal bipyramidal with N(2), Cl(1) and Cl(2) occupying the equatorial plane and N(1) and N(3) in the axial positions. For a trigonal bipyramid, the equatorial plane is formed by two Cl anions and N(2), consequently the two angles are close to the theoretical value of 120°. The Zn–N distances are averaged with the value of 2.189(9)Å. A section of the overall 3D hydrogen bonded network is shown in Fig. S1. The 3D structure has chlorine ions interspersed with the hydrogen of benzene. There is one type of face-to-face π–π stacking interaction apparent at a ring centroid separation of 3.382 Å.

3.2. Circular dichroism studies

CD spectroscopy is useful in monitoring the conformational variations of DNA in a solution and provides detailed information about the binding of the complex with DNA. The CD spectrum of CT-DNA exhibits a positive band at 275 nm due to base stacking and a negative band at 245 nm due to helicity, which is characteristic of DNA in the right-handed B form [64]. Fig. S2 displays the CD spectra of CT-DNA in the absence and presence of complexes **1**–**6**. Both the positive (~275 nm) and negative (~245 nm) bands decrease significantly in intensity with redshift with the addition of the complex. This suggests that the DNA-binding of the complexes induces certain conformational changes, such as the conversion from a more B-like to a more Z-like structure within the DNA molecule [65]. The CD spectroscopic results reveal that the complexes bind to CT-DNA effectively.

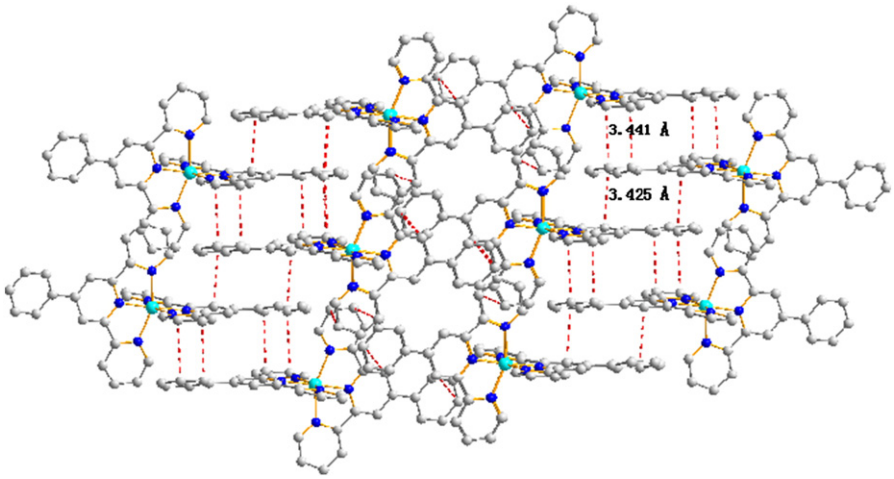

Fig. 4. The π-stacking overlap packing diagram of **3**. Hydrogen atoms and environmental anions are omitted for clarity.

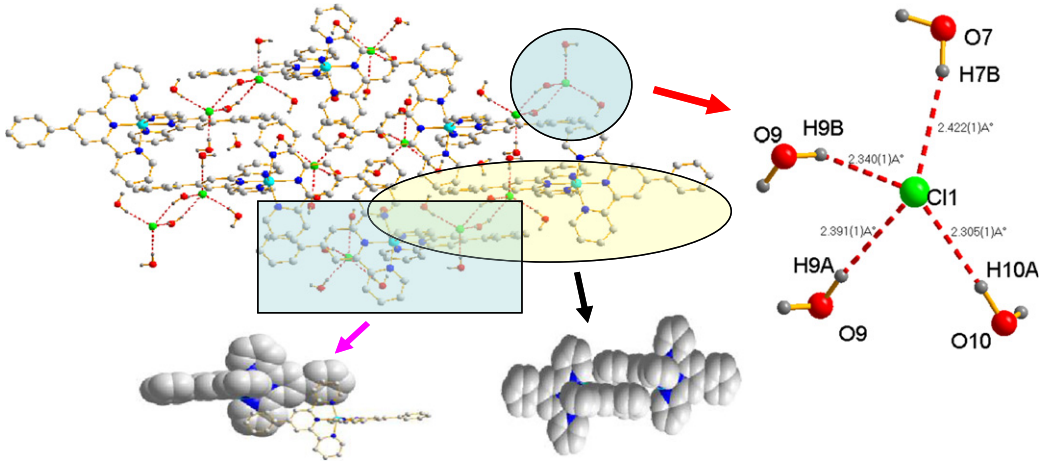

Fig. 5. Packing diagram of **4**. Hydrogen bonding network of Cl–H–C and ligand interactions.

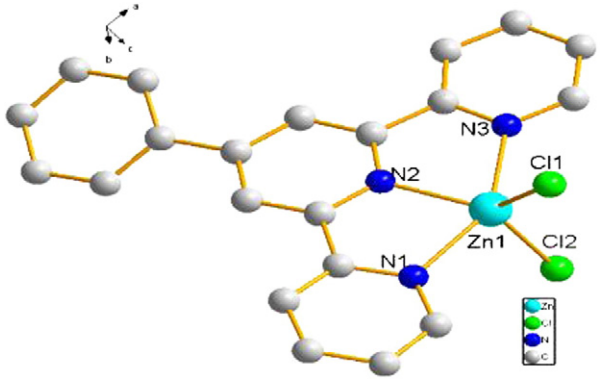

Fig. 6. Perspective view of **6** cation with the atom-numbering scheme.

3.3. UV–visible spectra

The complexes have a strong charge transfer absorption band in 282 nm assigned as intra-ligand electronic spectral transitions as shown in Fig. 7. The absorption intensity is consistent with the number of single-electron in the complexes.

3.4. DNA binding studies

The binding of the complexes to CT-DNA has been studied by an electronic absorption spectral technique. Binding of a complex to DNA through intercalation usually results in hypochromism and redshift (bathochromic shift) due to the intercalative mode involving a strong stacking interaction between the planar aromatic chromophore and the base pairs of DNA [66]. The extent of the hypochromism in the charge transfer band is commonly consistent with the strength of intercalative binding interaction. The absorption spectral traces of the complexes with increasing concentration of CT-DNA are shown in Fig S3. We have observed a minor bathochromic shift along with significant hypochromicity. When the amount of CT-DNA is increased, a decrease of about 30% in the intensity of the charge transfer band is observed. In order to compare the binding strength of the complexes, their intrinsic binding constants (K_b) with CT-DNA have been determined from the decay of the spectral band absorbance using Eq. (1) [67,68], where ε_a, ε_b and ε_f are the apparent absorption coefficient, ε_a of the metal complex in its free form and ε_a of the complex in its fully DNA-bound form, respectively. The intrinsic binding constant (K_b) values are given in Table 3.

$$[DNA]/(_a-\varepsilon_f) = [DNA]/(_b-_f) + 1/[K_b(_b-\varepsilon_f)] \quad (1)$$

The K_b values follow the order **1** > **4** > **3**, **5**, **2**, **6**. The high-spin complex **1** of the d^5 metal shows comparatively higher binding propensity to CT-DNA possibly due to an extended more unpaired d electrons than the other metals.

The binding of the complexes to the CT-DNA has also been studied by a fluorescence spectral method using the emission intensity of EB as a probe. EB in a buffer medium shows reduced emission intensity due to quenching by the solvent molecules. However, it shows significantly enhanced emission intensity when bound to DNA. Binding of the complex to DNA either displaces EB thus decreasing its emission intensity or quenching could take place due to the metal complexes in a DNA bound form. We have measured the reduction of the emission intensity of EB at different complex concentrations. According to the classical Stern–Volmer equation $I_0/I = 1 + K$ [Q]; I_0 and I are the fluorescence intensities in the absence and presence of the quencher, respectively. K is a linear Stern–Volmer quenching constant. [Q] is the concentration of the quencher. The quenching plots (ESI Fig. S4.) illustrate that the quenching of EB bound to DNA by complexes is in agreement with the linear Stern–Volmer equation [69], which also indicates that the complexes bind to DNA. In the plot of I_0/I vs. the concentrations of complexes, K is given by the ratio of the slope to the intercept. According to the equation K_{EB} [EB] = K_{app} [complex], where the complex concentration was the value at a 50% reduction of the fluorescence intensity of EB and $K_{EB} = 1.0 \times 10^7$ M^{-1}, ([EB] = 4.0 μ M). The K_{app} value is calculated to be 2.00×10^5, 2.75×10^5, 1.43×10^5, 1.37×10^5, 3.68×10^5 and 2.74×10^5 M^{-1} for complexes **1**–**6**, respectively, less than the binding constant of the classical intercalators and metallointercalators (10^7 M^{-1}), which suggests that the interaction of those complexes with DNA is a moderate intercalative mode.

3.5. pBR322 DNA cleavage activity by the complexes

Control cleavage experiments using pBR322 supercoiled DNA with the six complexes show no efficient DNA cleavage activity in the dark or in ambient light but show cleavage activity in UV-A light (365 nm) for **1**, **3**, and **4**. Complex **2** shows DNA cleavage activity in the presence of H_2O_2. Complexes **5** and **6** show no DNA photocleavage activity even in the presence of the UV-A light of 365 nm and hydrogen peroxide (H_2O_2). The concentration-dependent DNA cleavage in UV-A light shows that the cleavage activity increases with increasing complexes **1**–**4** and the percentage of undamaged binding sites has almost no change for **5** and **6** (Fig. S5). The Mn(II) complex (**1**) (a 10 μM solution) in UV-A light (ESI Fig. S5) for 3 h exhibits 97% cleavage of SC DNA (Fig. S5, (**1**) lane 6). The Ni(II) complexes **3** and **4** show moderate DNA photocleavage activity of 62% and 88%, respectively (Fig. S5, (**3**) lane 6 and (**4**) lane 6). The Fe(II) complex (**2**) is a relatively poor cleaver of DNA in UV-A light.

To verify if reactive oxygen species (ROS) may be formed in the DNA cleavage reaction, the photo-induced DNA cleavage reactions of the complexes have been studied in the presence of an additive under

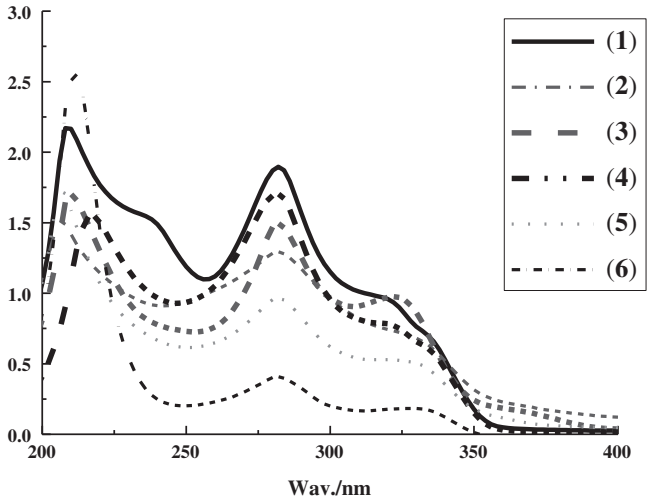

Fig. 7. UV–visible spectrum of **1**–**6** in DMF (5%) and H_2O (95%).

Table 3
Change in spectral features of the complexes on interaction with CT-DNA in 50 mM Tris–HCl/18 mM NaCl buffer (pH = 7.2).

Complex	Change in absorptivity	λ_{max} (nm)	$\Delta\lambda_{max}$ (nm)	Δε (%)	K_b
1	Hypochromism	206	2	58.65	1.91×10^5
2	Hypochromism	206	8	34.80	4.13×10^3
3	Hypochromism	208	10	30.49	7.64×10^3
4	Hypochromism	208	8	22.32	3.22×10^4
5	Hypochromism	206	10	31.72	7.42×10^3
6	Hypochromism	212	6	38.90	1.60×10^3

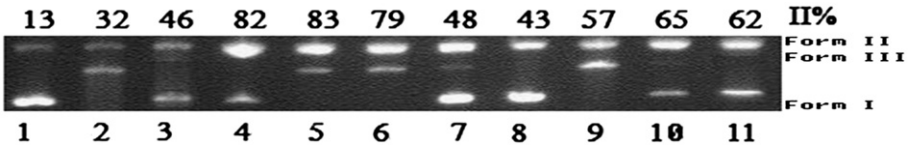

Fig. 8. Agarose gel showing cleavage of pBR322 DNA (0.1 μg/μL) incubated with complex **1** in Tris–HCl/NaCl buffer (pH = 7.2) at 37 °C for 30 min with irradiation at 365 nm. Lane 1: DNA control; lane 2: DNA + **1** (15 μM); lane 3: DNA + **1** (15 μM) + DMSO (100 μM); lane 4: DNA + **1** (15 μM) + NaN_3 (100 μM); lane 5: DNA + **1** (15 μM) + SOD (100 μM); lane 6: DNA + **1** (15 μM) + catalase (100 μM); lane7: DNA + **1** (15 μM) + KI (100 μM); lane 8: DNA + **1** (15 μM) + EDTA (100 μM); lane 9: DNA + **1** (15 μM) + D_2O (100 μM); lane 10: DNA + **1** (15 μM) + EtSH (100 μM); lane 11: DNA + **1** (15 μM) + histidine (100 μM).

UV-A light (365 nm). A series of control experiments were carried out using reagents like sodium azide and histidine as singlet oxygen ($^1O_2$) quencher; DMSO, EtSH, catalase and KI as hydroxyl radical scavengers; EDTA as chelating agent and superoxide dismutase (SOD) as an O_2^- radical scavenger. The mechanistic cleavage active in UV-A light is essentially the same for **1**–**4**. The present complexes are cleavage inactive in the dark indicating no apparent hydrolytic cleavage of DNA. Enhancement of the DNA cleavage in D_2O and inhibition in the presence of sodium azide or histidine suggest the possible involvement of singlet oxygen as the reactive species, and hydroxyl radical scavengers like DMSO, EtSH or KI also show partial inhibition in the DNA cleavage. The results suggest the involvement of both singlet oxygen and hydroxyl radicals as ROS. The chelating agent EDTA shows inhibition in the DNA cleavage (Figs. 8–11). The mechanistic data thus exclude the photoredox pathway superoxide radical ($O_2^{\bullet -}$) in the photocleavage reaction. The high spin d^5-Mn(II) complex (**1**) shows significant photo-induced DNA cleavage. The paramagnetic d^8-Ni(II) complexes (**3**) and (**4**) display moderate DNA cleavage activity in UV-A light. Low spin d^6-Fe(II) complex (**2**) shows poor DNA cleavage in the presence of hydrogen peroxide (H_2O_2) in UV-A light. Diamagnetic d^{10}-Zn(II) and d^{10}-Cd(II) complexes show inactive DNA cleavage even in the presence of hydrogen peroxide (H_2O_2) in UV-A light. The DNA photo-induced cleavage activity is consistent with the absorption intensity and the number of single-electron in metal of complexes.

4. Conclusions

In summary, a series of Phterpy complexes are prepared. Those complexes display binding propensity to the calf thymus DNA in the order: **1** > **4** > **3**, **5**, **2**, **6**. Control DNA cleavage experiments using pBR322 DNA with those complexes show no efficient DNA cleavage activity in the dark or in ambient light for the six complexes but show cleavage activity in UV-A light (365 nm) for high spin **1** d^5-Mn(II), **3** d^8-Ni(II), and **4** d^8-Ni(II) and show chemical nuclease activity in the presence of hydrogen peroxide (H_2O_2) for low spin **2** d^6-Fe(II). The **5** d^{10} Zn(II) and **6** Cd(II) complexes show inactive DNA photocleavage activity even in the light of 365 nm in the presence of hydrogen peroxide (H_2O_2). The mechanistic pathway involved the formation of singlet oxygen and hydroxyl radical as the reactive species. DNA cleavage activity studies show that the complexes examined here may be capable of promoting DNA cleavage with the selection of different metals. This work sets a good example of rational design of efficient photo-induced DNA cleavage nucleases.

5. Abbreviations

Phterpy	4′-phenyl-2,2′:6′,2″-terpyridine
DMF	*N*,*N*-dimethylformamide
EB	Ethidium bromide
CT-DNA	Calf thymus DNA
SOD	Superoxide dismutase
MTT	3-(4,5-Dimethylthiazol-2-yl)-2,5-diphenyltetrazolium bromide

Acknowledgments

This work was supported by the National Natural Science Foundation of China (nos. 21001066 and 21171101) and Reward Fund for Outstanding Young and Middle Aged Scientists of Shandong Province (no. 2012BSB01101) and Tianjin Science Foundation (no. 12JCYBJC13600).

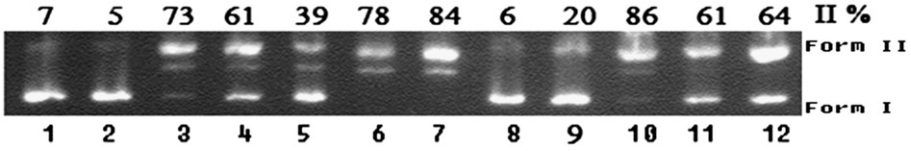

Fig. 9. Agarose gel showing cleavage of pBR322 DNA (0.1 μg/μL) incubated with complex **2** in Tris–HCl/NaCl buffer (pH = 7.2) at 37 °C for 30 min with irradiation at 365 nm. Lane 1: DNA control; lane 2: DNA + H_2O_2; lane 3: DNA + 2 (15 μM) + H_2O_2; lane 4: DNA + **2** (15 μM) + DMSO (100 μM) + H_2O_2; lane 5: DNA + **2** (15 μM) + NaN_3 (100 μM) + H_2O_2; lane 6: DNA + **2** (15 μM) + SOD (100 μM) + H_2O_2; lane 7: DNA + **2** (15 μM) + catalase (100 μM) + H_2O_2; lane8: DNA + **2** (15 μM) + KI (100 μM) + H_2O_2; lane 9: DNA + **2** (15 μM) + EDTA (100 μM) + H_2O_2; lane 10: DNA + **2** (15 μM) + D_2O (100 μM) + H_2O_2; lane 11: DNA + **2** (15 μM) + EtSH (100 μM) + H_2O_2; lane 12: DNA + **2** (15 μM) + histidine (100 μM) + H_2O_2.

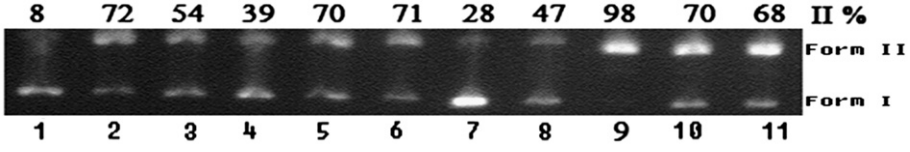

Fig. 10. Agarose gel showing cleavage of pBR322 DNA (0.1 μg/μL) incubated with complex **3** in Tris–HCl/NaCl buffer (pH = 7.2) at 37 °C for 30 min with irradiation at 365 nm. Lane 1: DNA control; lane 2: DNA + **3** (15 μM); lane 3: DNA + **3** (15 μM) + DMSO (100 μM); lane 4: DNA + **3**(15 μM) + NaN_3 (100 μM); lane 5: DNA + **3** (15 μM) + SOD (100 μM); lane 6: DNA + **3** (15 μM) + catalase (100 μM); lane7: DNA + **3** (15 μM) + KI (100 μM); lane 8: DNA + **3** (15 μM) + EDTA (100 μM); lane 9: DNA + **3** (15 μM) + D_2O (100 μM); lane 10: DNA + **3** (15 μM) + EtSH (100 μM); lane 11: DNA + **3** (15 μM) + histidine (100 μM).

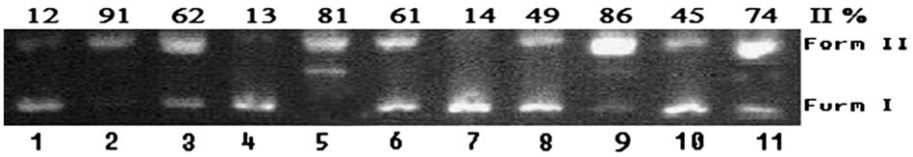

Fig. 11. Agarose gel showing cleavage of pBR322 DNA (0.1 μg/μL) incubated with complex **4** in Tris–HCl/NaCl buffer (pH = 7.2) at 37 °C for 30 min with irradiation at 365 nm. Lane 1: DNA control; lane 2: DNA + **4** (15 μM); lane 3: DNA + **4** (15 μM) + DMSO (100 μM); lane 4: DNA + **4** (15 μM) + NaN_3 (100 μM); lane 5: DNA + **4** (15 μM) + SOD (100 μM); lane 6: DNA + **4** (15 μM) + catalase (100 μM); lane7: DNA + **4** (15 μM) + KI (100 μM); lane 8: DNA + **4** (15 μM) + EDTA (100 μM); lane 9: DNA + **4** (15 μM) + D_2O (100 μM); lane 10: DNA + **4** (15 μM) + EtSH (100 μM); lane 11: DNA + **4** (15 μM) + histidine (100 μM).

Appendix A. Supplementary data

Electronic supplementary information (ESI) available

Packing diagram of [Zn(Phterpy)Cl_2] (**6**), hydrogen bonding network of Cl–H–C and ligand interactions (Fig. S1); the CD spectra of CT-DNA in the buffer solution (Fig. S2); absorption spectra of complexes **1**–**6** in the absence (dashed line) and presence (solid line) of increasing amounts of CT-DNA at room temperature in 50 mmol Tris–HCl/18 mmol NaCl buffer (pH = 7.2) (Fig. S3); fluorescence quenching curves and plots of I_0/I vs. [complex] of EB bound to DNA by complexes **1**–**6** (Fig. S4); gel electrophoresis diagrams showing the cleavage of pBR322 DNA at different concentrations (Fig. S5). Supplementary data associated with this article can be found, in the online version, at http://dx.doi.org/10.1016/j.jinorgbio.2013.01.010.

References

[1] H.T. Chifotides, K.R. Dunbar, Acc. Chem. Res. 38 (2005) 146–156.
[2] P.M. Bradley, A.M. Angeles-Boza, K.R. Dunbar, C. Turro, Inorg. Chem. 43 (2004) 2450–2452.
[3] P.J. Bednarski, F.S. Mackay, P.J. Sadler, Anticancer Agents Med Chem. 7 (2007) 75–93.
[4] P.J. Dyson, M.J. Rose, N.L. Fry, R. Marlow, L. Hinck, P.K. Mascharak, J. Am. Chem. Soc. 130 (2008) 8834–8846.
[5] P. Heringova, J. Woods, F.S. Mackay, J. Kasparkova, P.J. Sadler, V. Brabec, J. Med. Chem. 49 (2006) 7792–7798.
[6] E. Meggers, Chem. Commun. (2009) 1001–1010.
[7] V. Rajendiran, M. Palaniandavar, P. Swaminathan, L. Uma, Inorg. Chem. 46 (2007) 10446–10448.
[8] B. Rosenberg, L. VamCamp, J.E. Trosko, V.H. Mansour, Nature 222 (1969) 385–386.
[9] E.R. Jamieson, S.J. Lippard, Chem. Rev. 99 (1999) 2467–2498.
[10] F. Arnesano, G. Natile, Coord. Chem. Rev. 253 (2009) 2070–2081.
[11] A.V. Klein, T.W. Hambley, Chem. Rev. 109 (2009) 4911–4920.
[12] R. Gust, W. Beckb, G. Jaouenc, H. Schenberger, Coord. Chem. Rev. 253 (2009) 2742–2759.
[13] M. Skander, P. Retailleau, B. Bourri, L. Schio, P. Mailliet, A. Marinetti, J. Med. Chem. 53 (2010) 2146–2154.
[14] Z. Wu, Q. Liu, X. Liang, X. Yang, N. Wang, X. Wang, H. Sun, Y. Lu, Z. Guo, J. Biol. Inorg. Chem. 14 (2009) 1313–1323.
[15] Y. Jung, S.J. Lippard, Chem. Rev. 107 (2007) 1387–1407.
[16] K.S. Soppimath, L.H. Liu, W.Y. Seow, S.Q. Liu, R. Powell, P. Chan, Y.Y. Yang, Adv. Funct. Mater. 17 (2007) 355–362.
[17] Y. Xie, G.G. Miller, S.A. Cubitt, K.J. Soderlind, M.J. Allalunis-Turner, J.W. Lown, Anti-Cancer Drug Des. 12 (1997) 169–179.
[18] M. Shi, K. Ho, A. Keating, M.S. Shoichet, Adv. Funct. Mater. 19 (2009) 1689–1696.
[19] A. Hussain, D. Lahiri, B.M.S. Ameerunisha, S. Saha, R. Majumdar, R.R. Dighe, A.R. Chakravarty, Inorg. Chem. 49 (2010) 4036–4045.
[20] B.M.S. Mmeerunisha, S. Saha, M. Nethaji, A.R. Chakravarty, J. Inorg. Biochem. 104 (2010) 477–484.
[21] D. Lahiri, S. Roy, S. Saha, R. Majumdar, R.R. Dighe, A.R. Chakravarty, Dalton Trans. (2010) 1807–1816.
[22] P.K. Sasmal, S. Saha, R. Majumdar, R.R. Dighe, A.R. Chakravarty, Inorg. Chem. 49 (2010) 849–859.
[23] N. Raman, R. Jeyamurugan, A. Sakthivel, L. Mitu, Spectrochim. Acta, Part A 75A (2010) 88–97.
[24] S. Roy, S. Saha, R. Majumdar, R.R. Dighe, A.R. Chakravarty, Inorg. Chem. 48 (2009) 9501–9509.
[25] M. Roy, T. Bhowmick, R. Santhanagopal, S. Ramakumar, A.R. Chakravarty, Dalton Trans. (2009) 4671–4682.
[26] H.J. Yu, S.M. Huang, L.Y. Li, H.N. Jia, H. Chao, Z.W. Mao, J.Z. Liu, L.N. Ji, J. Inorg. Biochem. 103 (2009) 881–890.
[27] J.P. Nathan, Annu. Rep. Prog. Chem., Sect. A 104 (2008) 498–528.
[28] T.K. Goswami, M. Roy, M. Nethaji, A.R. Chakravarty, Organometallics 28 (2009) 1992–1994.
[29] M. Roy, T. Bhowmick, S. Ramakumar, M. Nethaji, A.R. Chakravarty, Dalton Trans. (2008) 3542–3545.
[30] P.K. Sasmal, A.K. Patra, A.R. Chakravarty, J. Inorg. Biochem. 102 (2008) 1463–1472.
[31] S. Roy, A.K. Patra, S. Dhar, A.R. Chakravarty, Inorg. Chem. 47 (2008) 5625–5633.
[32] M. Roy, B. Pathak, A.K. Patra, E.D. Jemmis, M. Nethaji, A.R. Chakravarty, Inorg. Chem. 46 (2007) 11122–11132.
[33] P.K. Sasmal, S. Roy, A.R. Chakravarty, Inorg. Chim. Acta 362 (2009) 1591–1599.
[34] S. Mondal, M. Mukherjee, K. Dhara, S. Ghosh, J. Ratha, P. Banerjee, A.K. Mukherjee, Cryst. Growth Des. 7 (2007) 1716–1721.
[35] S. Saha, A.K. Patra, M. Nethaji, A.R. Chakravarty, Inorg. Chem. 46 (2007) 4368–4370.
[36] M. Tanaka, K. Ohkubo, S. Fukuzumi, J. Am. Chem. Soc. 128 (2006) 12372–12373.
[37] M. Tanaka, K. Ohkubo, S. Fukuzumi, J. Phys. Chem. A 110 (2006) 11214–11218.
[38] F.S. Mackay, J.A. Woods, H. Moseley, J. Ferguson, A. Dawson, S. Parsons, P.J. Sadler, Chem. Eur. J. 12 (2006) 3155–3161.
[39] S. Dhar, M. Nethaji, A.R. Chakravarty, Inorg. Chem. 44 (2005) 8876–8883.
[40] P. Yang, Q. Yang, X.H. Qian, J.N. Cui, Bioorg. Med. Chem. 13 (2005) 5909–5914.
[41] S. Shi, J. Liu, J. Li, C. Kang, C.P. Tan, L.M. Chen, L.N. Ji, Dalton Trans. (2005) 2038–2046.
[42] A. Mukherjee, S. Dhar, M. Nethaji, A.R. Chakravarty, Dalton Trans. (2005) 349–353.
[43] M. Rajendran, R. Gandhidasan, R. Murugesan, J. Photochem. Photobiol. A 168 (2004) 67–73.
[44] H.P. He, T. Tian, P. Wang, L. Wu, J.J. Xu, X. Zhou, X.L. Zhang, X.P. Cao, X.J. Wu, Bioorg. Med. Chem. Lett. 14 (2004) 3013–3016.
[45] F.L. Tang, G. Yuan, J. Wang, Photochem. Photobiol. 78 (2003) 175–179.
[46] K. Toshima, R. Takano, T. Ozawa, S. Matsumura, Chem. Commun. (2002) 212–213.
[47] E.T. Farinas, J.D. Tan, P.K. Mascharak, Inorg. Chem. 35 (1996) 2637–2643.
[48] E.C. Constable, A.M.W. Cargill Thompson, D.A. Tocher, M.A.M. Daniels, New J. Chem. 16 (1992) 855–872.
[49] E.C. Constable, J. Lewis, M.C. Liptrot, P.R. Raithby, Inorg. Chim. Acta 178 (1990) 47–54.
[50] Y.Y. Kou, W. Gu, H. Liu, X.F. Ma, D.D. Li, S.P. Yan, Nankai Daxue Xuebao, Ziran Kexueban 41 (2008) 19–25.
[51] G.M. Sheldrick, Correction Software, University of Götingen, Germany, 1996.
[52] G.M. Sheldrick, SHELXS 97, Program for the Solution of Crystal Structures, University of Götingen, Germany, 1997.
[53] G.M. Sheldrick, SHELXL 97, Program for the Refinement of Crystal Structures, University of Götingen, Germany, 1997.
[54] J. Marmur, J. Mol. Biol. 3 (1961) 585–594.
[55] M.E. Reichmann, S.A. Rice, C.A. Thomas, P. Doty, J. Am. Chem. Soc. 76 (1954) 3047–3053.
[56] R.P. Herzberg, P.P. Derwan, J. Am. Chem. Soc. 104 (1982) 313–315.
[57] C.K. Mirabelli, C.H. Huang, S.T. Crooke, Cancer Res. 40 (1980) 4173–4177.
[58] C.A. Detmer, F.V. Pamatong, J.R. Borcarsly, Inorg. Chem. 35 (1996) 6292–6298.
[59] R.J.M. Klein Gebbin, R.T. Jonas, C.R. Goldsmith, T.D.P. Stack, Inorg. Chem. 41 (2002) 4633–4641.
[60] C.R. Goldsmith, A.P. Cole, T.D.P. Stack, J. Am. Chem. Soc. 127 (2005) 9904–9912.
[61] P. Guionneau, M. Marchivie, G. Bravic, J.F. Létard, D. Chassesu, Top. Curr. Chem. 234 (2004) 97–128.
[62] E.C. Constable, G. Baum, E. Bill, R. Dyson, R. Van Eldik, D. Fenske, S. Kaderli, D. Morris, A. Neubrand, M. Neuburger, D.R. Smith, K. Wieghardt, M. Zehnder, A.D. Zuberbuhler, Chem. Eur. J. 5 (1999) 498–508.
[63] J. McMurtriea, I. Dance, CrystEngComm 11 (2009) 1141–1149.
[64] A. Rajendran, B.U. Nair, Biochim. Biophys. Acta 1760 (2006) 1794–1801.
[65] A.D. Richards, A. Rodger, Chem. Soc. Rev. 36 (2007) 471–483.
[66] V.A. Bloomfield, D.M. Crothers, I.J. Tinocco, Physical Chemistry of Nucleic Acids, Harper & Row, New York, 1974, p. 432.
[67] J. Qian, W. Gu, H. Liu, F.X. Gao, L. Feng, S.P. Yan, D.Z. Liao, P. Cheng, Dalton Trans. (2007) 1060–1067.
[68] M. Navarro, C. Hernández, I. Colmenares, P. Hernández, M. Fernández, A. Sierraalta, E. Marchan, J. Inorg. Biochem. 101 (2007) 111–116.
[69] J.R. Lakowicz, G. Webber, Biochemistry 12 (1973) 4161–4170.